



University  
of Glasgow

Marsh, P., Manjakkal, L., Yang, X., Huerta, M., Le, T., Thiel, L., Chiao, J.-C., Cao, H. and Dahiya, R. (2020) Flexible iridium oxide based pH sensor integrated with inductively coupled wireless transmission system for wearable applications. *IEEE Sensors Journal*, (doi:10.1109/JSEN.2020.2970926).

There may be differences between this version and the published version. You are advised to consult the publisher's version if you wish to cite from it.

<http://eprints.gla.ac.uk/209106/>

Deposited on: 30 January 2020

Enlighten – Research publications by members of the University of Glasgow

<http://eprints.gla.ac.uk>

# Flexible Iridium Oxide based pH sensor Integrated with Inductively Coupled Wireless Transmission System for Wearable Applications

Paul Marsh, *Student Member, IEEE*, Libu Manjakkal, *Member, IEEE*, Xuesong Yang, *Student Member, IEEE*, Miguel Huerta, Tai Le, *Student Member, IEEE*, Lillian Thiel, *Student Member, IEEE*, J.-C. Chiao, *IEEE Fellow*, Hung Cao, *Senior Member, IEEE*, and Ravinder Dahiya, *IEEE Fellow*

**Abstract**— This work presents a pH sensor platform combining the high performance of iridium oxide (IrOx) fabricated by cyclic voltammetry with inductively-coupled wireless (ICW) transmission. Data included presents flexible potentiometric pH sensors having IrOx as the sensing electrode and a cured Ag/AgCl paste as the pseudo-reference electrode; further investigations concerning performance tailoring via fabrication processes are shown. The fabricated sensors show the best performance with a probe surface area of  $1 \times 1 \text{ mm}^2$ , electrodeposited for 100 cyclic voltammetry (CV) sweeps, at 100 mV/s. The sensitivity of the fabricated sensor is typically in the range of 65–75 mV/pH, as tested using either pH 4–9 (six points) or 2–10 (five points) buffers. The sensors exhibiting those sensitivities in buffer solutions yielded a response from “artificial sweat” solutions differing by  $\sim 0.4\text{--}0.8 \text{ pH}$  from a commercial glass pH electrode, while limit-of-quantification (LOQ) was measured to be  $\sim 0.04\text{--}0.08 \text{ pH}$ . The sensing electrode shows a response time of less than 2 seconds and minimal hysteresis effects. Cationic interferences from up to 1M  $\text{Na}^+$  resulted in  $+3\text{--}8 \text{ mV/pH}$  changes in sensitivity, depending on solution pH and probe, with minimal effects to LOQ. The performance under different bending conditions ( $0^\circ$ ,  $30^\circ$  at 55 mm radius,  $45^\circ$  at 37 mm, and  $90^\circ$  at 20 mm) of the flexible sensor probe show negligible variation. Finally, the presented sensors were integrated with an inductively coupled wireless (ICW) communication system for a demonstration of online monitoring. This sensor platform can easily be miniaturized due to a low count of necessary components and absence of onboard energy storage.

**Index Terms**— electrodeposition, iridium oxide, pH sensors, sweat monitoring, wearable, wireless system.

Paul Marsh, Miguel Huerta, Tai Le, and Lillian Thiel conducted all their work at the University of Washington Bothell campus. Paul Marsh, Tai Le, and Hung Cao finished writing of the manuscript at University of California Irvine. Lillian Thiel was financially supported by the 2017 NASA Summer Undergraduate Research Program. Paul Marsh, Miguel Huerta, and Tai Le were financially supported by National Science Foundation CAREER Award #1917105. Assistance from Scott Braswell, Gerry Hammer, and Dr. Micah Glaz at the Molecular Engineering & Sciences Institute, University of Washington. Part of this work was conducted at the Molecular Analysis Facility, a National Nanotechnology Coordinated Infrastructure site at the University of Washington which is supported in part by the National Science Foundation (grant ECC-1542101), the University of Washington, the Molecular Engineering & Sciences Institute, the Clean Energy Institute, and the National Institutes of Health. This work was partly supported in part by EPSRC Fellowship for Growth (EP/M002527/1 and EP/R029644/1) and North-West Centre for Advanced Manufacturing (H2020-Intereg-IVA5055) at Bendable

## I. INTRODUCTION

WITH a rising number of individuals with complex medical conditions, there is growing demand in the healthcare sector for innovative solutions enabling early detection of diseases. Wearable systems and smart clothing have attracted significant attention [4], as they are non-invasive, unobtrusive, and possibly enable health self-management [6, 7]. One important parameter is the pH of body fluids such as sweat [9], tears, wound fluid [11], and others. This is crucial for the diagnosis of several conditions such as diabetes [14, 15] and skin diseases [17]. See supplementary **Table S1** for a general comparison of wireless sweat pH probes.

Iridium Oxide (IrOx)-based sensors have shown promise as candidates for pH measurements in biological media due to excellent sensing performance across a wide pH range, reasonable linearity, fast and stable performance in different solution media, typically minimal interferences from ions and complex agents, and wide operating temperature ranges achievable without pre-treatment [18]. Sensors obtained using fabrication methods such as thermal oxidation [19], sputtering [20], sol-gel deposition [1], and anodic electrodeposition [21] have differing levels of probe sensitivity and stability. A comparison of these fabrication methods for is shown in **Table 1**. Anodic electrodeposition is distinct in terms of efficient yield, a room temperature (i.e. low energy) process possible on flexible substrates, high pH sensitivity (78–82 mV/pH) [22,

Electronics and Sensing Technologies (BEST) group, School of Engineering University of Glasgow, UK.

This work is an expansion of previous conference paper <https://ieeexplore.ieee.org/document/8589679>.

Paul Marsh, Tai Le, and Hung Cao are associated with Electrical Engineering, University of California Irvine, Irvine, CA, USA. Libu Manjakkal and Ravinder Dahiya are associated with Electronics and Nanoscale Engineering, University of Glasgow, G12 8QQ, Glasgow, Scotland, UK. Xuesong Yang is, and J.C. Chiao was, associated with Electrical Engineering, University of Texas at Arlington, Arlington, TX, USA. Paul Marsh, Miguel Huerta, Tai Le, and Hung Cao were associated with Electrical Engineering, University of Washington Bothell, Bothell, WA, USA. Lillian Thiel is associated with Electrical Engineering, University of Washington, Seattle, WA, USA. J.C. Chiao is associated with Electrical Engineering, Southern Methodist University, Dallas, TX, USA. Hung Cao is associated with Biomedical Engineering, University of California Irvine, Irvine, CA, USA.

TABLE I  
COMPARISON OF PERFORMANCE OF IrOx BASED pH SENSORS FABRICATED BY DIFFERENT METHODS

Fabrication method	Sensitivity (mV/pH)	pH range	Response Time	Application	Ref.
Dip coating	51.1	1.5-12	0.9 s for pH 3.9–11 2 s for pH 12-3.5	..	[1]
Carbonate-melt oxidation	58.4±0.2	1-13	--	...	[2]
Pechini method	59.1±1.47	1-13	120 s - pH 4-12 10 s - acidic region 5 s - basic region	...	[3]
Electrodeposition	72.9±0.9	3-11	--	Urea	[5]
Anodic electrodeposition	63.5±2.2	2-10	0.5, 1.5, and 1 min for pH regions <5, 5-7, and >7	Extracellular Myocardial Acidosis during acute Ischemia	[8]
Electrodeposition	77.9 (2-9)	2-9	..	..	[10]
Electrodeposition	47.5	4-8	..	Sweat	[12]
Carbonate-melt oxidation	56.7 ± 0.4	2-10	...	..	[13]
Electrodeposition	63.3	4-9.18	3- 5 min	bioanalytical	[16]
Electrodeposition	70 ± 5	4-9	< 2 s	Sweat	THIS WORK

23], and excellent pH sensing performance in biological media. However, deposition parameters and surface area influence sensing performance so a manufacturing investigation is demonstrated here.

In this work, we have developed a highly sensitive, electrodeposited, IrOx-based pH sensor integrated with a wireless communication system. Sensing performance with respect to deposition parameters was investigated. We fabricated a compact Ag/AgCl reference electrode (RE) on the same substrate; the IrOx sensor functioned as the sensing electrode (SE) in this potentiometric pair, where the open circuit potential (OCP) between the two served as the measurement. For wearable applications, the response was evaluated with an “artificial sweat” solution and compared to a commercial glass pH electrode. For real-time use, the sensor is integrated with an inductively coupled wireless (ICW) system. In previous literature, a wireless version of IrOx-based, CV-deposited pH sensors has already been demonstrated [24]. Moreover, a similar ICW system was demonstrated with pH sensing [25] but for use with sol-gel fabricated IrOx probes and

their lower sensitivity and in a different circuit configuration. In this work, an inductively-coupled power supply was utilized with a frequency-based load modulation scheme (LM) to both power the device and for backscattering communication.

## II. MATERIALS AND METHODS

The IrOx film was prepared by anodic electrodeposition. For this purpose, an iridium complex-containing aqueous solution was prepared using the recipe as originally intended for anodic electrodeposition of indium tin oxide by Yamanaka [21]. The exact preparation procedure is discussed in supplementary information section S1. A standard three-electrode cell (Fig. 1a) was used. A bare Au electrode was used as the substrate. The fabrication steps of the electrodes are shown in Fig. 1b and the details are described in supporting information, section S2. Voltammograms (Fig. 1c) depict the deposition current result from typical coating parameters (see supp. section S2). Increasing current maximums indicated IrOx film thickness growth [18] until peaking in the range of 85-120  $\mu\text{A}/\text{mm}^2$ . Electrodes were ramped at 100 mV/s between 0.7 and -0.8 V

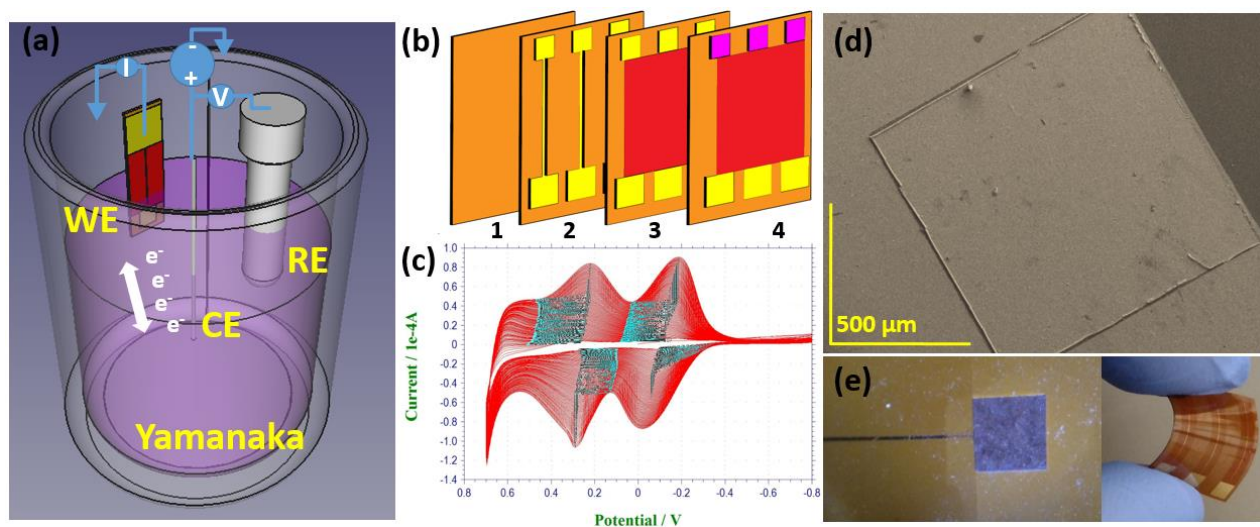


**Fig. 1.** Fabrication process. (a) 3-electrode electrodeposition cell used to create IrOx. (b) 3 stages of the lithography process, followed by IrOx deposition; (1) bare polyimide, (2) etched Au/Cr post lithography, (3) deposition of photoresist S1813 cover by spin coating, (4) IrOx electrodeposited onto Au. (c) Typical  $1 \times 1 \text{ mm}^2$  deposition cycle, 200 sweeps at 100 mV/s. (d) SEM image showing raised edge of deposited IrOx. (e) Sample images. Left- IrOx covered Au pad. Right- trio of probes, prior to IrOx electrodeposition;  $2 \times 2 \text{ mm}^2$  contact pads at the bottom,  $0.2 \times 0.2 \text{ mm}^2$  sensing pads at the top.

for 200 cycles.  $1 \times 1 \text{ mm}^2$  probes were also fabricated with 50–200 sweeps or 50–200 mV/s sweep rates. All parameter test results are shown in **Fig. S6**. Altering the sweep number caused maximum cathodic and anodic current densities to vary with some proportionality; charge density rates held at between 0.9 to  $1.0 \text{ } \mu\text{A}$  per sweep. A nearly linear relationship was seen between cathodic activation voltage and sweep number, varying at a rate of roughly  $-0.4 \text{ mV}$  per sweep. Anodic activation voltage had a less linear relationship, though stepping from 100 to 200 sweeps saw an increase of  $0.3 \text{ mV}$  per sweep (see supp. **Table S3**). Sweep speed proved to have a less pronounced and/or linear effect on both current densities ( $0.6$ – $1.5 \text{ } \mu\text{A}/\text{sweep}$ ) and activation voltages (little change). Pairs of electrodes were produced during each sweep number test, while single electrodes were prepared from the sweep rate tests. One probe from each sweep number pair was pH bath calibrated, while another was run through SEM/EDS analysis to observe surface morphology (see supp. **Fig. S11**). Finally, to achieve complete pH microprobes, micro REs were fabricated on the Au base. AgCl paste was used to form the pseudo-reference electrode (see **Fig. S3** and supp. section **S2**). Pseudo-RE's were placed in a potassium chloride (KCl) solution for 24–72 hours to observe their hydration responses, measured by OCP.

Probes were calibrated using multiple pH buffers while monitoring the resultant potential (hardware shown in **Fig. S4**) between the fabricated IrOx SE and a fabricated or commercial RE. For each measurement, the probe and the RE were placed in a buffer and the potential was allowed to settle, approximately 30 to 60 seconds. The probe was dipped in DI water between baths and gently dried with a thin cellulosic wipe (*Kimwipe, Kimberly Clark, Irving, TX*). To check performance over a wide range, two different panels were used: one comprised of commercial baths of pH 2, 4, 7, 9, and 10 (**Table S2**) and the other baths of pH 4, 5, 6, 7, 8, and 9. The pH 4, 7 and 9 baths were commercial, while the pH 5, 6 and 8 baths were dilutions. The 6-point panel was used after the pH 2 buffer in the 5-point panel was found to be highly damaging to the probes. As an aside, Britton-Robinson buffers were attempted with IrOx probes based on the ratios shown in [26]; results are briefly mentioned in this text. The hardware used for sensor characterization is described in supporting information. Selectivity, i.e. cationic interference, was determined by testing probes in pH buffers mixed with different concentrations of NaCl. Individual solutions were prepared in three pH levels (pH 4, 7, and 10) and six different molarities (0M, 0.1M, 0.2M, 0.4M, 0.6M, and 1M NaCl), for a total of 18 baths. Before testing in those baths, each probe was hydrated in DI water for 10 minutes. The probe potential was allowed to stabilize in each solution, the probe was rinsed in DI, and then the probe was moved to the next molarity within the same pH level until all were exhausted. A National Instruments USB DAQ unit was used for measurement purposes. Upon completion of the measurement panel, the probes were stored dry. An “artificial sweat” solution was prepared and tested; the solution comes from methods explained elsewhere [27] (section **S4** for composition). Prior to testing, a commercial probe was used to determine the exact pH level's deviation from the intended 6.5.

Before immersion, each probe was calibrated in the 6-point pH buffer panel to determine the final pH measurement in “sweat” solution; from the calibration ratio determined earlier, the “indicated” pH of the probe was calculated and compared to the commercial probe's most recent reading. Mechanically induced electrical errors were examined by performing panel calibrations while bending the sensors under angles of  $0^\circ$ ,  $30^\circ$ ,  $45^\circ$  and  $90^\circ$ , with radii of curvature of infinite, 55 mm, 37 mm, and 20 mm, respectively. Fixtures were designed in FreeCAD ([www.freecadweb.org](http://www.freecadweb.org)) and printed using polylactic acid (PLA) filament (*3D Solutech, Seattle, WA*). Parameters were hand-calculated for the results shown herein. Sensitivity was calculated as the slope of a least square linear regression of the probe's pH-potential relationship. From the raw temporal data, limit of quantification (LOQ) [1, 28] was calculated as

$$LOQ = \frac{(3 * \text{pH } 7 \text{ potential standard deviation})}{\text{calibrated sensitivity}} \quad (1)$$

which assumes a Gaussian distribution of noise about the signal mean. Hysteresis was calculated as the difference in potential between subsequent samplings of the same pH buffer in consecutive tests (5 – 15 minutes of immersion in buffer ranges listed above). In a typical experiment, the panel was sampled 3 times in linear order from pH 2 to pH 10, OCP was recorded for each, maximum OCP differentials were calculated for each discrete pH value, and this set of differentials was averaged across the pH range; while it is known that IrOx is more redox-active in certain pH ranges, averaging across the pH range was used here to limit the experiment's scope. Order-induced hysteresis was not investigated. Response time was determined to be the average settling time of probes [29] deposited into the “artificial sweat” solution.

The inductively coupled, frequency based LM circuit, for power and communication, used a 1 MHz sinusoid passed between planar antennas which the device side modulated with a square wave in the range of tens of kHz. The pH probe's potential is sent through a voltage buffer and used as an input to a voltage-controlled oscillator (VCO), which in turn controls a MOSFET tied to the input sinusoid and a reference voltage level. The resulting modulation was measured by oscilloscope after being passed through an envelope detector. This device is shown in **Fig. S5**. Calibration via wireless link was accomplished using the same procedure and 6-point buffer panel as that of typical parameter gathering.

### III. RESULTS, DISCUSSION, AND CONCLUSIONS

From **Table 1**, we are already aware that some deposition methods can create electrodes with super-Nernstian sensitivity. **Fig. 2a** shows the response of a sample set of five sensors fabricated with a surface area of  $1 \times 1 \text{ mm}^2$ , produced with 100 sweeps at  $100 \text{ mV/s}$ , exhibiting a super-Nernstian average of  $67.5 \text{ mV/pH}$ , ranging from 62.6 to  $71.5 \text{ mV/pH}$ ; a 99% confidence interval for  $n = 32$  sensors yields sensitivity of  $70 \pm 2 \text{ mV/pH}$  in the range of pH 2–10 (**Tables S6** and **S7**). In Britton-Robinson buffers, excellent preservation of the probe surface and reasonable sensitivity values were found but standard residuals revealed a notable and consistent bias in basic mixes, negating its use here. For other probes, the

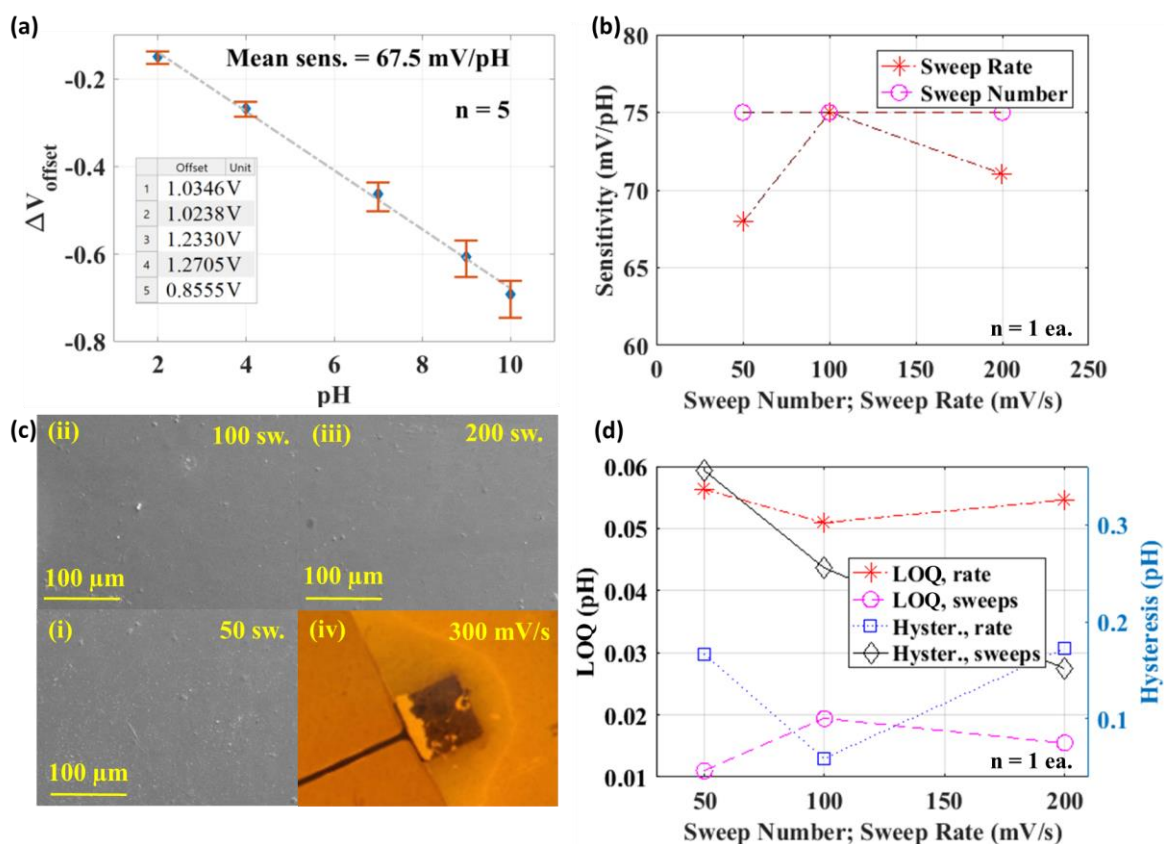


**Fig. 2.** Probe performance as explored through modification of deposition parameters. (a) Probe calibration example data as taken against a commercial glass reference electrode. All recorded values have been subtracted from the y-intercept of a least-squares linear regression from their datasets, in order to normalize the readings across probes. Voltage values were recorded from  $n = 5$  samples across different batches (surface area =  $1 \times 1 \text{ mm}^2$ ) using the same 5-pt buffer panel. This demonstrates the typical super-Nernstian response achieved with these probes. (b) Sensitivity, within a single batch, as related to varying sweep rates or sweep numbers. For sweep number tests, sweep rate used was  $100 \text{ mV/s}$ ; for sweep rate tests,  $100$  sweeps were performed. Each test features  $n = 1$  samples, for a total  $n = 6$  samples. (c) SEM images of surface change with reference to sweep number. Panels i, ii, and iii represent  $50$ ,  $100$ , and  $200$  sweeps, respectively (at  $100 \text{ mV/s}$ ). Panel iv demonstrates a probe failure at the extreme sweep rate of  $300 \text{ mV/s}$ . (d) LOQ and hysteresis, within a single batch, as related to varying deposition sweep rates or sweep numbers. Again,  $100 \text{ mV/s}$  sweeps were performed when varying sweep number and  $100$  sweeps were performed when varying sweep rate. Again, each test features an  $n = 1$  sample, for a total  $n = 6$  samples.

observed super-Nernstian response is due to the fact that more than one electron per proton was transferred in bulk redox reactions occurring in the electrode [30]. The generated potential between the SE and RE strongly affects the kinetics of reactions occurring on the IrOx surface. In addition to the ion exchange mechanism, a redox reaction also occurred on the SE. As the SE has been deposited on top of a conducting substrate (Au), an electrochemical capacitive double layer (ECDL) is formed by  $\text{H}^+$  and/or  $\text{OH}^-$  ions from solution, accumulating at the interface of IrOx/electrolyte [31]. Changes in pH level, then, lead to ion exchanges ( $\text{H}^+/\text{OH}^-$ ) in the surface layer of IrOx electrode film [32]. A Faradaic reaction occurs which involves electron transfer across the solution/oxide surface. This leads to a redox reaction which will happen throughout the IrOx. It is assumed that this intercalation of ions affects the stoichiometry of the solid phase IrOx, thereby also changing its redox state [33]. It has been theorized that this ion intercalation and redox state change alters the local hydrogen content because further protons are released when acid-base equilibrium is shifted in the bulk material, thus allowing potentials higher than Nernstian theory predicts. In addition to this, the Nernstian response of the IrOx-based pH sensor depends on fabrication method, owing itself mainly to the

resulting stoichiometry and crystalline structure of the material [34]. It has been found that SE's prepared by sputtering or thermal method have sensitivity close to the ideal Nernstian response ( $59 \text{ mV/pH}$ ) due to anhydrous iridium oxide formation [1, 19]; however, the SE prepared by electrodeposition shows "super-Nernstian" response due to the formation of hydrated iridium oxides [32-34]. Some SEM and XPS analysis of these surfaces can be found in the supplemental materials.

Sensitivity is strongly influenced by deposition parameters, including area [35] of the electrode. We carried out an investigation of the influence on sensing performance via (i) number of deposition sweeps, (ii) sweep rate, and (iii) surface area of the electrode. In our previous reports, we showed that sensors with surface areas of  $0.5 \times 0.5 \text{ mm}^2$ ,  $0.3 \times 0.3 \text{ mm}^2$ , and  $0.2 \times 0.2 \text{ mm}^2$  demonstrate mean sensitivities of  $61.6 \text{ mV/pH}$ ,  $52.2 \text{ mV/pH}$ , and  $50.7 \text{ mV/pH}$ , respectively [35]. For the batch used in this work, the baseline  $1 \times 1 \text{ mm}^2$  sensitivity was  $70.6 \text{ mV/pH}$ . Lowering of sensitivity due to decreased surface area was met with a commensurate rise in LOQ; the three smaller surface areas produced LOQs of  $0.047 \text{ pH}$ ,  $0.065 \text{ pH}$ , and  $0.075 \text{ pH}$ , respectively. For the batch used in this work, the baseline  $1 \times 1 \text{ mm}^2$  LOQ was  $0.040 \text{ pH}$  (Fig. S8). This is likely due to a change in proton diffusion area [18], or a relation between

surface area and oxygen evolution [33]. LOQ changes may be due to capacitance changes [18]. Since capacitance is also related to area, reductions in area (i.e. reductions in capacitance) may be “tuning” the lead/probe to different frequencies of ambient noise. Measured sensitivity, as it relates to sweep rate and sweep number, is shown in **Fig. 2b**. Calibration sensitivity is not related to sweep count (confirming other work [18]); probes were equal to within 1 mV/pH of each other when tested together. Increasing sweep counts, i.e. increasing deposition thickness, smoothed the surface substantially (**Fig. 2c**, panels **i**, **ii**, and **iii**). Sweep rate did cause a minor change in sensitivity (**Fig. 2b**). **Fig. 2c**, panel **iv** demonstrates a pad wherein deposition was attempted at scan rates of 300 mV/s and expanded voltages of  $\pm 2$  V; 50  $\mu\text{m}$  traces and Au flakes delaminate. Best performance came from 100 mV/s and 200 sweeps (**Fig. 2d**). It is possible that the 100 mV/s sweep rate discussed previously is ideal due to a decrease in redox reaction rates when thicker films inhibit electron movement [36]. According to Yamanaka [21], thin films of different physical appearance could be produced by alternating between anodic and cathodic current; in more recent work, authors have reported that anodic and cathodic currents result in alternation between oxidation states of iridium [25, 37]. This has the effect of reducing and re-oxidizing the outer layer of iridium complexes being formed, as this has been reported to

be a reversible redox couple, thus allowing for linear control of film thickness [37]. Improvements in LOQ and hysteresis given higher sweep numbers would seem to indicate that there is a surface morphology relationship at play. Hidalgo-Acosta et al. previously theorized that Ir oxide stoichiometry changes with changes in acid-base equilibria at the metallic film surface [23], which is supportive of our previous experience in super-Nernstian behavior seen in large probe sizes. A similar mechanism may be at work in the variability of our LOQ/hysteresis with respect to sweep count, as we may be seeing minor surface area changes with decreasing roughness. Possibly, these roughness changes are altering sensitivity along with LOQ and hysteresis, just to a much smaller degree than changes in pad size (and to a smaller degree than is detectable here); further study is warranted. Response time of the sensor was measured as the time required for its potential to reach 90% of an equilibrium value after a drastic changing of the pH value of solution ( $t_{90}$ ), from acidic to basic and vice versa. The sensor showed a very fast response of less than 2 s after each pH change.

Flexible micro RE's were fabricated on the Au base. Stability was tested by immersion into a KCl solution potential vs a commercial RE was measured at a 1 Hz acquisition rate for up to 5 days. The data was passed through a low pass filter with an  $f_c = 1.5$  Hz, then a moving average filter with a window of

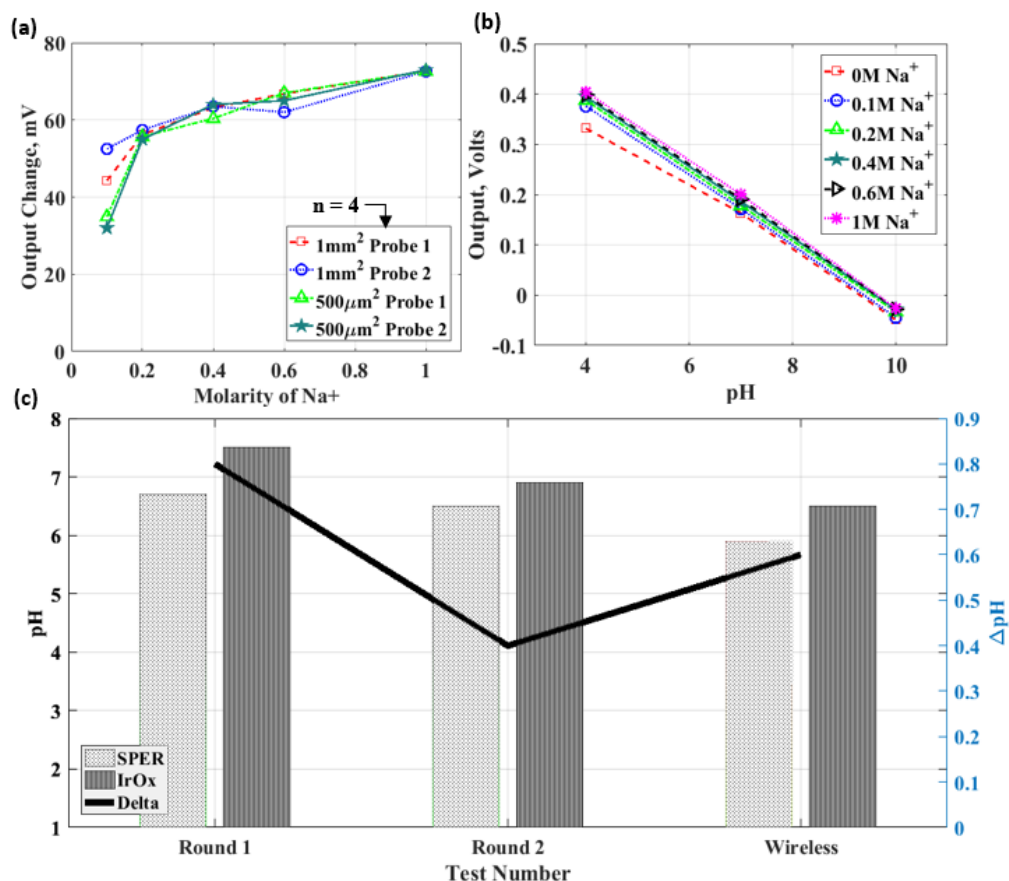


**Fig. 3.** Interference and applicability testing. (a) Highlighted potential variation of IrOx probe readings, from four probes, in pH 4 solution with varying molarities of added Na<sup>+</sup>; deltas are between the tested molarity and neutral solutions with 0M Na<sup>+</sup>. (b) Full data, potential of an IrOx probe as passed through baths of three pH levels and six different Na<sup>+</sup> molarities. (c) “Artificial sweat” solution test, three different runs. Round 1 and Round 2 represent tests of the solution several weeks apart, featuring both a commercial pH meter and wired acquisition of IrOx probes.

60 samples (results in **Fig. S9a**). Each pseudo-RE encountered a large potential swing (approximately 40 mV); these particular REs all experienced this swing at ~17 hours after immersion. After this, the RE saw a potential variation of no more than  $\pm 3$  mV, though some linear reduction did continue. After multiple rounds of testing, physical inspection of the probes revealed (**Fig. S11**) locations where the AgCl paste had completely separated from the Au substrate. The potentiometric sensing performance of the fabricated pseudo-REs were investigated with relation to IrOx based SEs. The sensor pairs exhibit sensitivities of  $67 \pm 2$  mV/pH with a typical  $R^2 \approx 0.98$  for their regression fits. The observed sensitivity of the paste-based RE is lower than the sensitivity measured using a glass RE. The probes were typically used immediately after fabrication, without a hydration step. In this work, the RE lacks the KCl layer that a conventional glass-based RE has and it will influence potential [38]. Nernstian potentials measured against the commercial RE did not repeat with custom RE's possibly due to paste phase changes. Following Cranny and Atkinson [39], a modified version of the Nernst equation applies here:

$$E = E^0 - 2.303 \left( \frac{RT}{nF} \right) \log_{10}(\text{Cl}^-)^\alpha \quad (2)$$

In Eq. 2,  $E$  = cell potential,  $E^0$  = standard cell potential,  $R$  = the universal gas constant,  $T$  = cell temperature,  $n$  = number of electrons transferred ( $n$  assumed 1 here),  $F$  = Faraday's constant, and  $\alpha$  = ion activity. The factor changing here is  $\alpha$ , the Cl ion activity. In a commercial RE, the Cl ion activity is near-unity due to the surrounding medium; this may not be the case with the pseudo-RE's since their hydration process could be causing  $\text{Cl}^-$  separation or mixing in the bulk paste [38, 40].

To test potential variations in "artificial sweat", two different batches of probes were calibrated (one set of three probes in the 5-point buffer panel, one set of three probes in the 6-point panel) and used to measure the pH of an "artificial sweat" solution as compared to a commercial glass pH probe (#840087, SPER Scientific, Scottsdale, AZ), which itself had been two-point calibrated to pH buffers; the two-point calibration consisted of setting the potential offset with a commercial pH 7 buffer and then setting the slope using either a commercial pH 2 or 10 buffer, depending on which baths were being measured. Calibration of the pH probes in the first batch revealed sensitivities of 72.3, 72.5, and 72.6 mV/pH; batch two probes were found to have sensitivities of 72.1, 72.3, and 65.6 mV/pH. To ensure parity for this test, the probe with 65.6 mV/pH sensitivity was not used. Probe performance is shown in **Fig. 3c**. Each bar grouping represents the comparison of the SPER (SPER Scientific, Scottsdale, AZ) commercial pH probe reading versus the average reading of the probe batch. This simulates the delta in accuracy between a highly selective probe and a bare metallic probe. The solution appeared to acidify over time and the Ir probes always read a more basic pH than the glass probe; batch 1 measured high by 0.79 pH, while batch 2 measured high by 0.36 pH. Standard deviations of the batch results were 0.041 pH and 0.014 pH, respectively. Therefore, the "accuracy" of the probes versus commercial probes is  $\sim 0.4 - 0.8$  pH, while the "precision" of the probes is  $\sim 0.04 - 0.08$  pH. The deltas of  $0.4 - 0.8$  pH to the commercial probe can be

an issue; as noted in [11], a typical range between healthy skin and wounds are, at a minimum, 1 pH, and can be as much as 2.5 pH. We acknowledge that our maximum delta to commercial probes nears this minimum healthy/wound difference but other literature suggests that healthy skin pH alone can vary 0.7 pH with age and body location [41], and may be  $> 1$  pH in certain populations [42]. Therefore, precision (LOQ) would be of higher importance in these scenarios. We expect worst case LOQs of 0.08 pH to be sufficient for this task. All of these combined reveals that, even in cation-containing solutions, the proposed sensor is still super-Nernstian in its sensitivity and linear regressive fits have low enough error for most applications, therefore being applicable in wearable sweat monitoring. The electrochemical performance of the sensor under the influence of different concentration of  $\text{Na}^+$  ions was monitored, using buffers of pH 4, 7, and 10 with NaCl salt concentrations of 0M, 0.1M, 0.2M, 0.4M, 0.6M, and 1M. This testing was performed in two rounds to attempt to negate the effects of sensor fabrication variability and surface area: first, a batch of four probes, two with the sensing area of  $0.5 \times 0.5$  mm<sup>2</sup> and two with  $1 \times 1$  mm<sup>2</sup>, chosen at random, were tested roughly 1 month after fabrication. Second, a batch of  $1 \times 1$  mm<sup>2</sup> size probes, chosen at random, one freshly fabricated and one having been calibrated in the 6-point panel, were tested roughly 1 month after fabrication. **Figs. 4a** and **4b** show typical sensor performance under various  $\text{Na}^+$  ions concentration and varying pH levels. For the purposes of this test, probes were calibrated before use and found to have initial sensitivities varying from  $\sim 60$ - $69$  mV/pH. In the presence of  $\text{Na}^+$  ions the sensor shows a drift in sensitivity ( $+3$ - $8$  mV/pH, with one outlier differing a maximum of  $+14.7$  mV/pH) as compared to the sensor performance in normal buffer solution; the sensitivity change is mainly due to heightened potential offsets in more acidic conditions. No obvious correlation between sensitivity and magnitude of ionic interference was detected.

To confirm the bendability of the SE, the device was bent at angles of  $0^\circ$ ,  $30^\circ$ ,  $45^\circ$ , and  $90^\circ$  during calibration. These featured radii of curvature of infinite, 55 mm, 37 mm, and 20 mm, respectively. They were adhered to fixtures printed from polylactic acid filament, as shown in **Figs. S10a**, **S10b**, and **S10c**. Results are shown in **Figs. S10d** and **S10e**. With mechanical bending, the sensors showed sensitivity changes of 0.7 to 2.1 mV/pH and LOQ changes of  $-0.001$  to  $0.007$  pH. The effect, therefore, was considered negligible.

For the LM circuit (**Fig. 4c**), probe voltages were monitored with a wired system at the same time their potential was being converted to frequency and recorded. With initial passive components around the VCO, a 62.4 mV/pH probe was found to have a linear correlation coefficient of  $R^2 = 0.999$  by wired acquisition and 0.993 by LM transmission; a 67.8 mV/pH probe was found to have  $R^2 = 0.999$  by wired acquisition and 0.977 by wireless acquisition. Wireless and wired outputs for these two probes are shown in **Figs. 5a** and **5b**, respectively. It was assumed that some of this deviation from linear fit was due to manual measurement error, so the frequency range was lowered into the single kHz range and averaging was performed with the frequency counter after envelope detection (typically 15–25 one

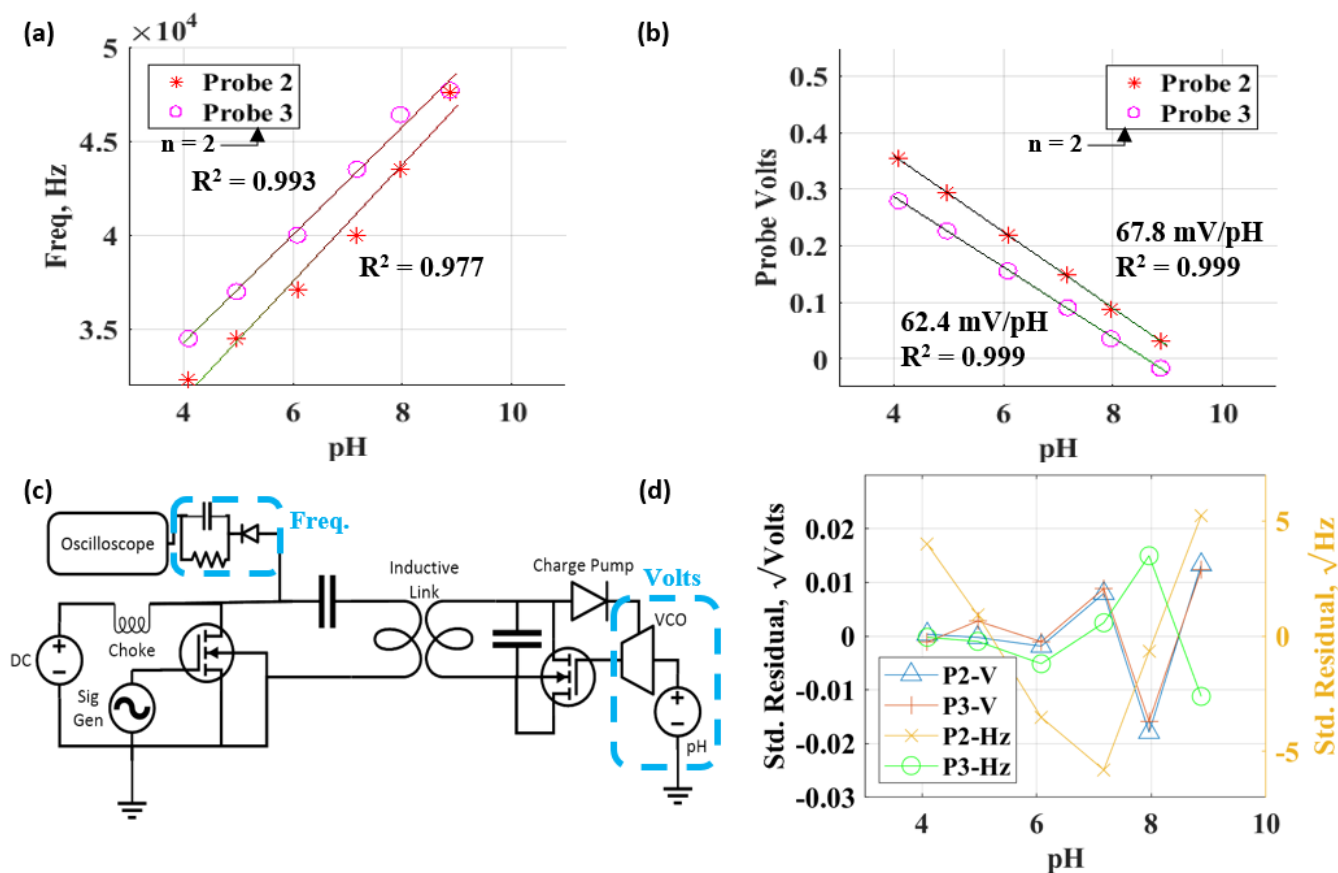


**Fig. 4.** Schematic and calibration results from the LM scheme. (a) Calibration results for two probes are shown, as resulting from the envelope detector. (b) Calibration output frequencies are shown from those same two probes, as resulting from VCO modulation. (c) Schematic of the load modulation circuit. On the left side, a sinusoidal output is generated and transmitted across an inductive link; the receiving side then mixes this signal with a modulation resulting from a pH-controlled oscillator. That modulation is passed through an envelope detector on the transmitting side to discern a frequency resulting from a given pH reading. (d) Standard residuals as calculated from the linear regressive fits of (a) and (b).

second averages). After this adjustment, a 60.3 mV/pH probe was found to have an  $R^2$  of 0.999 by wired acquisition and 0.999 by LM transmission. **Fig. 4d** shows standard residuals for the voltage- and frequency-based signals. The more basic potential measurements do show some consistent, though zero-centered, non-linearity, as expected. More random residuals from the frequency signals suggest the same voltage bias had been convoluted with measurement precision after the envelope detector. Maximum error from linear regressive fits was calculated to be 0.08 pH for the wired configuration and 0.38 pH for the wireless configuration, average errors were 0.03 pH (wired) and 0.16 pH (wireless). The wireless configuration features a higher maximum and average regressive fit error than the wired configuration but both values are still smaller than the measurement delta to the commercial reference; while future tuning of the circuit to improve this accuracy is preferable, its current configuration is viable.

#### IV. FUTURE WORK

In our future work, we plan to investigate the long-term stability of sensors in real body fluid samples such as wound fluid, urine, sweat and saliva. With appropriate electrode coatings, this device can potentially be used to investigate a range of biologic conditions, including wound health, implant condition, and metabolic processes, not to mention ecological

applications for clean drinking water and the like. Some probe degradation occurred in testing, so attempting to reduce IrOx grain edge area, or miniaturizing grains to match substrate strain, may help reduce hysteresis in future sensors; membrane coatings coupled with cation selectivity tests will be performed in future work. As an aside, interested audiences can find selectivity enhancements in the form of ion-selective coatings and “sentinel” sites for signal subtraction demonstrated in literature [43, 44].

#### REFERENCES

- [1] W.-D. Huang, H. Cao, S. Deb, M. Chiao, and J.-C. Chiao, "A flexible pH sensor based on the iridium oxide sensing film," *Sensors and Actuators A: Physical*, vol. 169, pp. 1-11, 2011.
- [2] M. Wang, S. Yao, and M. Madou, "A long-term stable iridium oxide pH electrode," *Sensors and Actuators B: Chemical*, vol. 81, pp. 313-315, 2002.
- [3] G. Da Silva, S. Lemos, L. Pocrifka, P. Marreto, A. Rosario, and E. Pereira, "Development of low-cost metal oxide pH electrodes based on the polymeric precursor method," *analytica chimica acta*, vol. 616, pp. 36-41, 2008.
- [4] M. Stoppa and A. Chiolerio, "Wearable electronics and smart textiles: a critical review," *sensors*, vol. 14, pp. 11957-11992, 2014.
- [5] E. Prats-Alfonso, L. Abad, N. Casañ-Pastor, J. Gonzalo-Ruiz, and E. Baldrich, "Iridium oxide pH sensor for biomedical applications. Case urea-urease in real urine samples," *Biosensors and Bioelectronics*, vol. 39, pp. 163-169, 2013.
- [6] D. Metcalf, S. T. Milliard, M. Gomez, and M. Schwartz, "Wearables and the internet of things for health: Wearable, interconnected

- devices promise more efficient and comprehensive health care," *IEEE pulse*, vol. 7, pp. 35-39, 2016.
- [7] O. Amft, "How wearable computing is shaping digital health," *IEEE Pervasive Computing*, vol. 17, pp. 92-98, 2018.
- [8] S. A. Marzouk, S. Ufer, R. P. Buck, T. A. Johnson, L. A. Dunlap, and W. E. Cascio, "Electrodeposited iridium oxide pH electrode for measurement of extracellular myocardial acidosis during acute ischemia," *Analytical chemistry*, vol. 70, pp. 5054-5061, 1998.
- [9] W. Dang, L. Manjakkal, W. T. Navaraj, L. Lorenzelli, V. Vinciguerra, and R. Dahiya, "Stretchable wireless system for sweat pH monitoring," *Biosensors and Bioelectronics*, vol. 107, pp. 192-202, 2018.
- [10] S. Shahrestani, M. Ismail, S. Kakooei, M. Beheshti, M. Zabihiazadboni, and M. Zavareh, "Iridium Oxide pH Sensor Based on Stainless Steel Wire for pH Mapping on Metal Surface," in *IOP Conference Series: Materials Science and Engineering*, 2018, p. 012014.
- [11] L. A. Schneider, A. Korber, S. Grabbe, and J. Dissemmond, "Influence of pH on wound-healing: a new perspective for wound-therapy?," *Archives of dermatological research*, vol. 298, pp. 413-420, 2007.
- [12] M. Zamora, J. Dominguez, R. Trujillo, C. Goy, M. Sanchez, and R. Madrid, "Potentiometric textile-based pH sensor," *Sensors and Actuators B: Chemical*, 2018.
- [13] Y. Pan, Z. Sun, H. He, Y. Li, L. You, and H. Zheng, "An improved method of preparing iridium oxide electrode based on carbonate-melt oxidation mechanism," *Sensors and Actuators B: Chemical*, 2018.
- [14] J. Moyer, D. Wilson, I. Finkelshtein, B. Wong, and R. Potts, "Correlation between sweat glucose and blood glucose in subjects with diabetes," *Diabetes technology & therapeutics*, vol. 14, pp. 398-402, 2012.
- [15] H. Lee, C. Song, Y. S. Hong, M. S. Kim, H. R. Cho, T. Kang, *et al.*, "Wearable/disposable sweat-based glucose monitoring device with multistage transdermal drug delivery module," *Science advances*, vol. 3, p. e1601314, 2017.
- [16] S. Bause, M. Decker, F. Gerlach, J. Näther, F. Köster, P. Neubauer, *et al.*, "Development of an iridium-based pH sensor for bioanalytical applications," *Journal of Solid State Electrochemistry*, vol. 22, pp. 51-60, 2018.
- [17] M.-H. Schmid-Wendtner and H. C. Körtling, "The pH of the skin surface and its impact on the barrier function," *Skin pharmacology and physiology*, vol. 19, pp. 296-302, 2006.
- [18] H. A. Elsen, C. F. Monson, and M. Majda, "Effects of electrodeposition conditions and protocol on the properties of iridium oxide pH sensor electrodes," *Journal of The Electrochemical Society*, vol. 156, pp. F1-F6, 2009.
- [19] S. Yao, M. Wang, and M. Madou, "A pH electrode based on melt-oxidized iridium oxide," *Journal of the electrochemical society*, vol. 148, pp. H29-H36, 2001.
- [20] T. Katsube, I. Lauks, and J. Zemel, "pH-sensitive sputtered iridium oxide films," *Sensors and Actuators*, vol. 2, pp. 399-410, 1981.
- [21] K. Yamanaka, "Anodically electrodeposited iridium oxide films (AEIROF) from alkaline solutions for electrochromic display devices," *Japanese journal of applied physics*, vol. 28, p. 632, 1989.
- [22] I. A. Ges, B. L. Ivanov, D. K. Schaffer, E. A. Lima, A. A. Werdich, and F. J. Baudenbacher, "Thin-film IrO<sub>x</sub> pH microelectrode for microfluidic-based microsystems," *Biosensors and Bioelectronics*, vol. 21, pp. 248-256, 2005.
- [23] J. C. Hidalgo-Acosta, M. D. Scanlon, M. A. Méndez, V. Amstutz, H. Vrabel, M. Opallo, *et al.*, "Boosting water oxidation layer-by-layer," *Physical Chemistry Chemical Physics*, vol. 18, pp. 9295-9304, 2016.
- [24] S. Anastasova, B. Crewther, P. Bembnowicz, V. Curto, H. M. Ip, B. Rosa, *et al.*, "A wearable multisensing patch for continuous sweat monitoring," *Biosensors and Bioelectronics*, vol. 93, pp. 139-145, 2017.
- [25] W.-D. Huang, S. Deb, Y.-S. Seo, S. Rao, M. Chiao, and J. Chiao, "A passive radio-frequency pH-sensing tag for wireless food-quality monitoring," *IEEE Sensors Journal*, vol. 12, pp. 487-495, 2012.
- [26] J. E. Reynolds III, M. Josowicz, P. Tyler, R. B. Vegh, and K. M. Solntsev, "Spectral and redox properties of the GFP synthetic chromophores as a function of pH in buffered media," *Chemical Communications*, vol. 49, pp. 7788-7790, 2013.
- [27] C. Callewaert, B. Buyschaert, E. Vossen, V. Fievez, T. Van de Wiele, and N. Boon, "Artificial sweat composition to grow and sustain a mixed human axillary microbiome," *Journal of microbiological methods*, vol. 103, pp. 6-8, 2014.
- [28] A. B. Amar, H. E. Amor, H. Cao, and A. B. Kouki, "Fabrication of LTCC micro-fluidic devices for wireless Lab-On-A-Chip applications," *Additional Papers and Presentations*, vol. 2016, pp. 000085-000088, 2016.
- [29] P. R. Dahiya, "Engineering Fellowship for Growth - Neuromorphic Printed Tactile Skin (NeuPRINTSKIN) (Ext)," ed. University of Glasgow: Engineering and Physical Sciences Research Council, 2018.
- [30] P. VanHoudt, Z. Lewandowski, and B. Little, "Iridium oxide pH microelectrode," *Biotechnology and bioengineering*, vol. 40, pp. 601-608, 1992.
- [31] L. Manjakkal, W. Dang, N. Yogeswaran, and R. Dahiya, "Textile-Based Potentiometric Electrochemical pH Sensor for Wearable Applications," *Biosensors*, vol. 9, p. 14, 2019.
- [32] W. Olthuis, M. Robben, P. Bergveld, M. Bos, and W. Van Der Linden, "pH sensor properties of electrochemically grown iridium oxide," *Sensors and Actuators B: Chemical*, vol. 2, pp. 247-256, 1990.
- [33] P. Steegstra and E. Ahlberg, "Influence of oxidation state on the pH dependence of hydrous iridium oxide films," *Electrochimica Acta*, vol. 76, pp. 26-33, 2012.
- [34] M. Khalil, S. Wang, J. Yu, R. L. Lee, and N. Liu, "Electrodeposition of Iridium Oxide Nanoparticles for pH Sensing Electrodes," *Journal of The Electrochemical Society*, vol. 163, pp. B485-B490, 2016.
- [35] P. Marsh, W. Moore, M. Clucas, L. Huynh, K.-T. Kim, S. Yi, *et al.*, "Characterization of Flexible pH micro-Sensors Based on Electrodeposited IrO<sub>x</sub> Thin Film," in *IEEE Sensors*, Glasgow, Scotland, 2017.
- [36] L. D. Burke and D. Whelan, "A voltammetric investigation of the charge storage reactions of hydrous iridium oxide layers," *Journal of electroanalytical chemistry and interfacial electrochemistry*, vol. 162, pp. 121-141, 1984.
- [37] J. Hu, M. Abdelsalam, P. Bartlett, R. Cole, Y. Sugawara, J. Baumberg, *et al.*, "Electrodeposition of highly ordered macroporous iridium oxide through self-assembled colloidal templates," *Journal of Materials Chemistry*, vol. 19, pp. 3855-3858, 2009.
- [38] M. Sophocleous and J. K. Atkinson, "A review of screen-printed silver/silver chloride (Ag/AgCl) reference electrodes potentially suitable for environmental potentiometric sensors," *Sensors and Actuators A: Physical*, 2017.
- [39] A. Cranny and J. K. Atkinson, "Thick film silver-silver chloride reference electrodes," *Measurement Science and Technology*, vol. 9, p. 1557, 1998.
- [40] L. Manjakkal, D. Shakthivel, and R. Dahiya, "Flexible Printed Reference Electrodes for Electrochemical Applications," *Advanced Materials Technologies*, vol. 3, p. 1800252, 2018.
- [41] K.-P. Wilhelm, A. B. Cua, and H. I. Maibach, "Skin aging: effect on transepidermal water loss, stratum corneum hydration, skin surface pH, and casual sebum content," *Archives of dermatology*, vol. 127, pp. 1806-1809, 1991.
- [42] M. Man, S. Xin, S. Song, S. Cho, X. Zhang, C. Tu, *et al.*, "Variation of skin surface pH, sebum content and stratum corneum hydration with age and gender in a large Chinese population," *Skin pharmacology and physiology*, vol. 22, pp. 190-199, 2009.
- [43] H. Cao, A.-L. Li, C. M. Nguyen, Y.-B. Peng, and J.-C. Chiao, "An integrated flexible implantable micro-probe for sensing neurotransmitters," *IEEE Sensors Journal*, vol. 12, pp. 1618-1624, 2011.
- [44] K. N. Hascup, E. R. Hascup, F. Pomerleau, P. Huettl, and G. A. Gerhardt, "Second-by-second measures of L-glutamate in the prefrontal cortex and striatum of freely moving mice," *Journal of Pharmacology and Experimental Therapeutics*, vol. 324, pp. 725-731, 2008.